Self-Consistent Properties of Carbon Nanotubes and Hexagonal Arrays as Composite Reinforcements

R. Byron Pipes[a], S.J.V. Frankland[b], Pascal Hubert[c] and Erik Saether[d]

[a]The University of Akron, Polymer Engineering Academic Center, Akron, OH 44325-0301
[b]ICASE, NASA Langley Research Center, Hampton, VA 23681
[c]McGill University, Montreal, Quebec, H3A 2K6
[d]NASA Langley Research Center, Hampton, VA 23681

Keywords: single wall carbon nanotubes, density, modulus, hexagonal array, volume fraction, weight fraction, composites

1.0 Abstract

A self-consistent set of relationships is developed for the physical properties of single walled carbon nanotubes (SWCN) and their hexagonal arrays as a function of the chiral vector integer pair, (n,m). Properties include effective radius, density, principal Young's modulus, and specific Young's modulus. Relationships between weight fraction and volume fraction of SWCN and their arrays are developed for the full range of polymeric mixtures. Examples are presented for various values of polymer density and for multiple SWCN diameters.

2.0 Introduction

The use of single walled carbon nanotubes (SWCN) for reinforcement of polymeric materials has been given as one of the primary applications for this new material form since its discovery more than a decade ago [1]. Yet no unified basis for reporting the physical properties of SWCN or arrays of SWCN as reinforcements has emerged. For example, the reference volume, required to measure volume dependent properties, is taken as the entire cylindrical volume enclosed by the carbon atom crystal lattice when reporting density [2], while for the effective Young's modulus, the cylindrical volume with inner and outer diameter defined by the bounds of the monoatomic layer of carbon atoms is used [3, 4]. These different geometry definitions have led to reported axial moduli ranging from 1.25 Tpa [4] for SWCN to 67 GPa [7] in arrays. The need for a self-consistent set of properties is evident. Another author [5] has also stated this need, but does not offer a set of relationships that unify these data. In order to account for the contribution of the SWCN to the overall properties of the polymeric composite wherein the SWCN serves the role of the reinforcement, it is necessary to view its effective properties so that they correspond to a specified volume within the composite. In this work, the representative volume element for all physical properties is defined as that of a cylindrical volume with diameter equal to twice the effective SWCN radius, where the effective SWCN radius includes one-half the van der Waals equilibrium separation distance.

The van der Waals equilibrium distance for SWCN can be defined as the average center-to-center distance between the carbon atom of the SWCN and the nearest atom of the

adjacent medium. Therefore, the van der Waals standoff distance is dependent upon the properties of the adjacent medium. In the case of an array composed of SWCN of equal diameter, the individual SWCN are surrounded by other SWCN of like properties and the equilibrium distance is designated as λ. Suspension of SWCN in a polymeric phase yields a different separation distance, ν. When employing the equations developed in the present work, it is necessary to establish the value of ν corresponding to the suspending medium which can vary widely. In this paper, the equilibrium separation distance in polymers is assumed to be 0.342 nm, the equilibrium separation distance for graphene sheet [14]. The SWCN and SWCN array physical property predictions presented in the present work include density, principal Young's modulus (longitudinal direction) and specific modulus. It is common practice to refer to weight fraction when determining properties of mixtures of SWCN and secondary polymeric phase even though the physical properties of the mixture depend upon the volume fractions of the constituents. In the present work, relationships are developed not only to predict the physical properties of the SWCN and its arrays, but also to predict relationships that are necessary to convert SWCN weight fraction to volume fraction in mixtures. These property relationships then serve to provide precursor data for computational methods in the prediction of effective properties of SWCN composites.

The literature is filled with reported values for the Young's modulus of carbon nanotubes and their arrays [6-10]. These reported values differ by almost two orders of magnitude. The SWCN density has also been reported [12,13]; however, no clear methodology for density calculation has been published in the literature.

It is the objective of this paper to develop a self-consistent set of properties for the SWCN and its hexagonal arrays and to provide the mixing rules for conversion of weight fraction to volume fraction for mixtures of SWCN and SWCN arrays with polymers. Properties predicted include effective radius, density, principal Young's modulus, and specific Young's modulus.

3.0 SWCN Geometry

The SWCN has been described as a single graphene sheet rolled up with varying degrees of twist as described by its chiral vector, $\mathbf{C_h}$ [14]:

$$\mathbf{C_h} = n\mathbf{a_1} + m\mathbf{a_2} \tag{1}$$

where $\mathbf{a_1}$ and $\mathbf{a_2}$ are unit vectors in the two-dimensional hexagonal lattice and the chiral vector, $\mathbf{C_h}$ is also referred to by its indices, n and m. Nanotubes with chiral vectors of (n,n) and (n,0) have no twist and are classified as chiral nanotubes. These two special cases are sometimes denoted "armchair" and "zig zag," respectively, referring to the pattern of the carbon atoms around the nanotube circumference[14]. Geometric representations of SWCN structures of three different chiralities are shown in Figure 1. These images illustrate the dependence of the SWCN upon the components of the chiral vector, (n,m). The SWCN radius, R_n as shown in Figure 2 is given in the following relation as a function of the integer pair and the C-C bond length, b [14]:

$$R_n = \frac{b}{2\pi}\sqrt{3}\Lambda \tag{2}$$

where

$$\Lambda = \sqrt{\left(n^2 + m^2 + mn\right)} \tag{3}$$

For the SWCN, the C-C bond length, b is equal to 0.142 nm [14]. The carbon nanotube structure as shown in Figure 2a is replaced by the effective reinforcing element in Figure 2b.

The diameter $2R_n$ of the SWCN is a strong function of the chiral integers n and m and varies over a wide range as shown in Table 1. However, it is the smaller diameters of SWCN that are of most interest as a polymeric reinforcement since the transverse properties of the larger tube diameters can lead to their collapse [15]. The remaining geometric descriptors of the SWCN are the cross-sectional area and length. As stated earlier, several investigators have taken the SWCN equilibrium separation distance to be equal to that of the equilibrium separation distance of graphene sheets of 0.342 nm [15]. This issue requires more discussion since, as stated earlier, the cross-sectional area occupied by the SWCN is influenced by the character of the adjacent medium.

Table 1 SWCN Diameter for Various Chiral Integers.

n	m	$2R_n$ (nm)
5	5	0.68
4	6	0.68
3	7	0.70
2	8	0.72
10	10	1.36
50	50	6.78
6	0	0.48
8	0	0.63
10	0	0.78
12	0	0.94

18	0	1.41
24	0	1.88
50	0	3.91
96	0	7.52

As in discontinuous fiber systems, the length of the SWCN is likely to be a function of the processing technologies used for both the carbon nanotubes and the incorporation of the polymeric phase. Bundle lengths of up to 20,000 nm have been measured [16,17].

The effective radius of the SWCN, R_{ne}, is defined as the radius given in equation (2), R_n, plus one-half the equilibrium separation distance between the SWCN and the polymer. By defining SWCN radius in this way, the total volume of the heterogeneous mixture is accounted for as follows:

$$R_{ne} = \frac{b}{2\pi}\sqrt{3}\Lambda + \frac{v}{2} \tag{4}$$

4.0 SWCN Hexagonal Array

The synthesis of SWCN typically results in the generation of collimated arrays of SWCN with hexagonal cross-sectional arrangement [17]. In the present study we examine the equilibrium separation distance, λ, of such a hexagonal array calculated using the methods discussed in reference [18], wherein the van der Waals interactions of the SWCN are modeled with the Lennard-Jones potential with ε=34.0 K and σ = 0.3406 nm [18]. The results for (n,0) SWCN were calculated in static molecular simulations and are presented in Table 2.

These results suggest that the separation distance is not a function of the SWCN diameter, but rather can be taken as a constant equal to 0.318 nm in agreement with the equilibrium distance of 0.313 nm determined in reference [19] and 0.315 nm in reference [20] for a similar range of SWCN diameters. Thus, the SWCN effective radius, R_{na}, in an array configuration (See Figure 3) is expressed as:

$$R_{na} = \frac{b}{2\pi}\sqrt{3}\Lambda + \frac{\lambda}{2} \tag{5}$$

The carbon nanotube array shown in Figure 3a is replaced by the effective reinforcement array shown in Figure 3b. For a constant separation distance, λ, the SWCN volume fraction of the hexagonal array, V_a, is a constant and is equal to the volume packing fraction of 0.906:

$$V_a = \frac{\pi}{2\sqrt{3}} = 0.906 \tag{6}$$

The hexagonal SWCN array can be considered as a reinforcement form similar to the individual SWCN. As such, the descriptions presented are for the effective properties of the array in the absence of a second phase.

Table 2 SWCN (n,0) Hexagonal Array Separation Distance.

n	Diameter (nm)	Separation Distance, λ (nm)
6	0.48	0.316
12	0.94	0.317
18	1.41	0.317
24	1.88	0.318
54	4.23	0.318
96	7.51	0.319

5.0 Density

The density of the SWCN in the present work is defined as the total mass of the carbon atoms in the enclosed volume as defined in equation (5). To calculate the mass of the carbon atoms, it is necessary to express their number per unit length, N in the nanotube representative volume element:

$$N = \frac{4\Lambda}{3b} \tag{7}$$

Then the nanotube density, ρ_n can be expressed in terms of the chiral vector by combining equations (4) and (7) as follows:

$$\rho_n = \frac{NM_w}{\pi N_a R_{ne}^2} = \frac{16\pi M_w \Lambda}{3N_a b\left(3b^2\Lambda^2 + 2\sqrt{3}b\pi\nu\Lambda + \pi^2\nu^2\right)} \tag{8}$$

where ν, measured in nm, is the equilibrium standoff distance between the SWCN and

the adjacent medium, M_w is carbon atomic weight and N_a is Avogadro's number. SWCN density as a function of diameter (equation 8) is presented in Figure 4 along with the specific values of chiral vector. Density is shown in tabular form in Table 3 over a range of chiral vectors. These results show that SWCN density decreases with increasing diameter by an order of magnitude over a range of diameters between 1 and 14 nanometers.

Table 3 SWCN Chiral Integers Versus Density

n	***m***	**Density, g/cm^3**
5	5	1.99
4	6	1.99
3	7	1.98
2	8	1.95
10	10	1.44
50	50	0.41
6	0	2.18
8	0	2.04
10	0	1.89
12	0	1.75
18	0	1.40
24	0	1.16
50	0	0.66
96	0	0.37

The results presented in Table 4 for a (10,10) SWCN show that density is a weak function of the choice of the van der Waals distance, ν. Nanotubes having other values of chiral vector also showed a similar weak dependence on ν.

Table 4 van der Waals Distance and Density for (10,10) SWCN

ν, nm	Density, g/cm^3
0.32	1.471
0.33	1.453
0.34	1.436
0.35	1.419
0.36	1.403

The density of the hexagonal array of SWCN is the product of the SWCN density in an array configuration (equations 5 and 7) and the volume packing fraction of the hexagonal array (equation 6):

$$\rho_a = V_a \rho_{na} = V_a \frac{NM_w}{\pi N_a R_{na}^2} = \frac{\pi}{2\sqrt{3}} \left[\frac{16\pi M_w \Lambda}{3N_a b\left(3b^2\Lambda^2 + 2\sqrt{3}b\pi\lambda\Lambda + \pi^2\lambda^2\right)} \right] \tag{9}$$

Like the density of the individual SWCN, the array density shows a significant reduction with SWCN diameter (equation 9). It is noteworthy that density of the SWCN array differs from that of the SWCN only by the product of the maximum volume fraction (0.906) and the difference in separation distances, ν and λ. Since the separation distances for the array (0.318 nm) and individual SWCN (0.342 nm) are similar, it is likely that the array density will not differ significantly from those of the SWCN. Figure 5 shows a comparison between density values for individual SWCN and arrays of SWCN for several nanotube chiralities.

6.0 Principal Young's Modulus

Here the principal modulus is taken as the modulus of the SWCN and its arrays in the direction parallel to the SWCN longitudinal axis. In the following development it is assumed that the SWCN are continuous and that the array consists of SWCN of identical diameter. The present model is a simplified approach wherein the stiffness of a graphene sheet, rolled into the SWCN configuration, is mapped onto the enclosed volume defined by the effective SWCN radius.

6.1 SWCN

The present approach to estimate the Young's modulus, E_n, of the SWCN is to represent the SWCN as a thin-walled cylinder of outer radius, R_{ne}, predicted by equation (4). It is assumed that the stiffness of the thin-walled cylinder representing the SWCN is equal to that of the Young's modulus of the graphene sheet, Y, and that the SWCN occupies the enclosed cylindrical volume. E_n and Y are given as:

$$E_n = \frac{8YR_n\nu}{4R_n^2 + 4R_n\nu + \nu^2}$$
$$Y = \frac{\left(C_{11}^2 - C_{12}^2\right)}{C_{11}} \tag{10}$$

where C_{11} and C_{12} are the stiffness constants of graphene [20].

Substituting equation (2) into (10) yields:

$$E_n = \frac{4\sqrt{3}\pi b Y \Lambda \nu}{3b^2\Lambda^2 + 2\sqrt{3}b\pi\Lambda\nu + \pi^2\nu^2} \tag{11}$$

Equation (11) shows that the modulus of the SWCN decreases with increasing radius. Earlier work described in references [7, 10, 11] has shown a similar behavior. Here the work described in [10] is compared with the present work predicted in equation (11)

$$E_n = \frac{A}{R_n} + B \tag{12}$$

where the constants in equation (12) are defined as A = 429.6 GPa-nm and B = 8.42 GPa and were obtained from [10]. The choice of the equilibrium separation distance, ν, and Young's modulus of the graphene sheet in equation (11) uniquely determine the quantitative values of the SWCN Young's modulus for all radii. In the present study, we take the experimental value of the Young's modulus of the graphene sheet as reported in reference [21] as 1029 GPa and the separation distance as that for the graphene sheet of 0.342 nm. Predictions of SWCN modulus as a function of diameter using equation (11) are shown in Figure 6. Table 5 illustrates the utility of equation (11) in determining Young's modulus for five specific sets of chiral integers, (n,m). In addition, a comparison with the results of references [7] and [11] show that all four models provide very similar results.

Table 5 SWCN Young's modulus for specific chiral integers.

n	*m*	E_n, GPa Eq. 11	E_n, GPa Eq. 12	E_n, GPa Ref. 7	E_n, GPa Ref.11
10	10	662	642	608	680
18	0	647	618	594	664
24	0	536	465	492	550
50	0	304	228	279	311
96	0	171	123	157	175

6.2 SWCN Hexagonal Array Extension

Utilizing the Young's modulus, E_{na}, of individual SWCN in an array configuration, we obtain the following SWCN array modulus:

$$E_a = V_a E_{na} = \frac{2\pi^2 bY\Lambda\lambda}{3b^2\Lambda^2 + 2\sqrt{3}b\pi\Lambda\lambda + \pi^2\lambda^2} \tag{13}$$

Results for the principal modulus of the SWCN array shown in Figure 7 and predicted by equation (13) show that the array modulus follows identical trends as for the individual SWCN. This is true because the two predictions differ only by the product of the maximum volume fraction (0.906) and the difference in van der Waals distances (λ = 0.318 for the array). Predictions of equation (13) also show excellent agreement with those presented in reference [20] obtained from lattice dynamics calculations for (3*n*,3*n*) "armchair" and (3*n*,0) "zigzag" SWCN as shown in Figure 7. The data taken from [20] were for four data points and one interpolated value. To further clarify the differences in

moduli between the SWCN and the array, results are presented in Figure 8 for several nanotube chiralities.

7.0 Specific Axial Modulus

The specific modulus, $E_{\rho n}$, of the SWCN is defined as the ratio of the principal Young's modulus, E_n, divided by a quantity analogous to specific gravity of the SWCN, $\overline{\rho}_n$. Combining equations (8) and (10) yields the expression:

$$E_{\rho n} = \frac{E_n}{\overline{\rho}_n} = \frac{3N_a\sqrt{3}b^2 Y\nu}{4M_w} \tag{14}$$

Equation (14) yields results independent of the SWCN diameter since the same SWCN volume is utilized in the calculation of both modulus and density.

In a similar manner, the specific modulus for the SWCN array, $E_{\rho a}$, is obtained by combining equations (9) and (13):

$$E_{\rho a} = \frac{E_a}{\overline{\rho}_a} = \frac{3N_a\sqrt{3}b^2 Y\lambda}{4M_w} \tag{15}$$

These results show that the specific modulus of the SWCN array is identical in form to that of the SWCN.

8.0 Weight Fraction Versus Volume Fraction

With the establishment of the density of the SWCN, it is now possible to develop a relationship between weight fraction and volume fraction of SWCN in a mixture with a

second material such as a polymer. Consider a SWCN/polymer mixture of density, ρ_m with a SWCN volume fraction, V_n, a SWCN density of ρ_n and a polymer density of ρ_p. The SWCN volume fraction can be expressed as follows:

$$V_n = \frac{\rho_m - \rho_p}{\rho_n - \rho_p} \tag{16}$$

It is also possible to express the SWCN volume fraction in terms of its weight fraction, W_n:

$$V_n = \frac{\rho_m}{\rho_n} W_n = \frac{W_n \rho_p}{W_n \rho_p + (1 - W_n)\rho_n} \tag{17}$$

Combining equations (20) and (8) we obtain the final expression for SWCN volume fraction:

$$V_n = \frac{W_n 3b\left(3b^2\Lambda^2 + 2\sqrt{3}b\pi\nu\Lambda + \pi^2\nu^2\right)\rho_p}{W_n \rho_p 3b\left(3b^2\Lambda^2 + 2\sqrt{3}b\pi\nu\Lambda + \pi^2\nu^2\right) + (1 - W_n)16\pi k\Lambda} \tag{18}$$

The relationship between volume fraction and weight fraction for SWCN-polymer mixtures is shown in Figure 9 for (6,6), (12,12) and (18,18) SWCN for a polymer density of 1 g/cm^3. These results show that as the diameter of the SWCN is decreased, the non-linearity in the relationship increases. This occurs because the difference between the SWCN and polymer densities increases as the SWCN diameter decreases. Results in the dilute concentration regime ($W_n < 0.012$) are shown in Figure 10 for convenience since many applications are in this range. The influence of variations in polymer density upon

the relationship between volume and weight fraction is shown in Figure 11 for the (10,10) SWCN. Here increasing polymer density decreases the non-linearity in the relationship. This occurs because as the polymer density increases from 0.8 to 1.2 g/cm^3, it approaches the density of the (10,10) SWCN which is 1.44 g/cm^3. Again, as the density difference between the polymer and SWCN decreases, the non-linearity in the weight fraction volume fraction is also decreasing.

The relationship for the volume fraction of SWCN arrays, V_a, in terms of the corresponding weight fraction ,W_a , for SWCN arrays in a polymer mixture is:

$$V_a = \frac{W_a 3\sqrt{3}b\left(3b^2\Lambda^2 + 2\sqrt{3}b\pi\nu\Lambda + \pi^2\lambda^2\right)\rho_p}{W_a\rho_p 3\sqrt{3}b\left(3b^2\Lambda^2 + 2\sqrt{3}b\pi\nu\Lambda + \pi^2\lambda^2\right) + \left(1 - W_a\right)8\pi^2 k\Lambda} \tag{19}$$

Figure 12 illustrates a similar weight-volume fraction relationship for SWCN arrays as was shown in Figure 9 for individual SWCN suspended in a polymeric phase of density 1 g/cm^3. Arrays in dilute concentrations suspended in a polymeric phase are illustrated in Figure 13 for (6,6), (12,12) and (18,18) SWCN. Finally, the influence of polymer density upon the relationship between polymer mixtures containing SWCN arrays is shown in Figure 14.

These relationships, based on a consistent definition of volume and thereby, volume fraction, are necessary for micromechanics calculations to determine the effective properties of nanotube reinforced polymers.

9.0 Summary Table of Properties

Table 6 shows the set of physical properties of the SWCN and its hexagonal arrays as a function of the chiral vector, (*n*,*m*).

10.0 Conclusions

The primary objective of this paper was to develop a consistent set of predictions for several of the physical properties of SWCN and their arrays to provide the foundation for developing an understanding of SWCN and arrays as reinforcements in polymers.

The density and moduli of the SWCN and the SWCN array are shown to differ only slightly since the van der Waals distances differ only modestly (0.318 nm versus 0.342 nm) and the SWCN array has a packing fraction of 0.906. The equilibrium separation distance for the SWCN array, determined to be 0.318 nm, was seen to be in good agreement with the values of 0.313 nm and 0.315 nm published earlier in the literature.

When the simple model for the SWCN principal modulus, consisting of a hollow cylinder with properties of the cylinder wall equal to the stiffness of the graphene sheet was employed, the specific modulus of both the SWCN and its SWCN arrays were found to be independent of SWCN diameter.

For both the SWCN and SWCN array, the principal Young's modulus showed significant dependence upon SWCN radius. Predictions of SWCN array principal moduli were also shown to be in excellent agreement with those previously published in the literature obtained from lattice dynamics calculations for (3n,3n) "armchair" and (3n,0) "zigzag" SWCN. Maximum principal modulus was achieved at the smallest SWCN radius, while

density decreased significantly for increased SWCN radius.

A useful equation was derived for the relationship between weight fraction and volume fraction for SWCN and SWCN arrays. The relationship requires knowledge only of the components of the chiral vector of the SWCN and the weight fractions of the constituents to determine volume fraction of the SWCN and SWCN arrays in a mixture.

11.0 Acknowledgements

This research was supported by the National Aeronautics and Space Administration under NASA Cooperative Agreement NCC-1-02002 and Contract No. NAS1-97046 while S. J. V. Frankland was in residence at ICASE, NASA Langley Research Center.

Table 6 Properties of SWCN and SWCN arrays.

Property	**SWCN**	**SWCN Array**
Radius (nm)	$R_{ne} = \frac{b}{2\pi}\sqrt{3}\Lambda + \frac{v}{2}$	$R_{na} = \frac{b}{2\pi}\sqrt{3}\Lambda + \frac{\lambda}{2}$
Density (g/cm^3)	$\rho_n = \frac{16\pi M_w \Lambda}{3bN_a\left(3b^2\Lambda^2 + 2\sqrt{3}b\pi v\Lambda + \pi^2 v^2\right)}$	$\rho_a = \frac{\pi}{2\sqrt{3}N_a}\left[\frac{16\pi M_w \Lambda}{3b\left(3b^2\Lambda^2 + 2\sqrt{3}b\pi\lambda\Lambda + \pi^2\lambda^2\right)}\right]$
Modulus (GPa)	$E_n = \frac{4\sqrt{3}\pi bY\Lambda v}{3b^2\Lambda^2 + 2\sqrt{3}b\pi\Lambda v + \pi^2 v^2}$	$E_{na} = V_a E_{na} = \frac{2\pi^2 bY\Lambda\lambda}{3b^2\Lambda^2 + 2\sqrt{3}b\pi\Lambda\lambda + \pi^2\lambda^2}$
Specific Modulus (GPa)	$E_{\rho n} = \frac{3\sqrt{3}b^2 Yv}{4k}$	$E_{\rho a} = \frac{3\sqrt{3}b^2 Y\lambda}{4k}$
Volume-Weight Fraction	$V_n = \frac{W_n 3b\left(3b^2\Lambda^2 + 2\sqrt{3}b\pi v\Lambda + \pi^2 v^2\right)\rho_p}{W_n\rho_p 3b\left(3b^2\Lambda^2 + 2\sqrt{3}b\pi v\Lambda + \pi^2 v^2\right) + (1-W_n)16\pi k\Lambda}$ $V_a = \frac{W_a 3\sqrt{3}b\left(3b^2\Lambda^2 + 2\sqrt{3}b\pi v\Lambda + \pi^2\lambda^2\right)\rho_p}{W_a\rho_p 3\sqrt{3}b\left(3b^2\Lambda^2 + 2\sqrt{3}b\pi v\Lambda + \pi^2\lambda^2\right) + (1-W_a)8\pi^2 k\Lambda}$	
	$\Lambda = \sqrt{\left(n^2 + m^2 + mn\right)}$ b = 0.142 nm ν = 0.342 nm Y = 1029 GPa	$M_w/N_a = 0.01995$ λ = 0.318 nm

11.0 References

1. Iijima, S., Nature, 354, 56 (1991).

2. Collins, P.G. and Avouris, P., "Nanotubes for Electronics," Scientific American, (December 2000), pp. 62-69.

3. Majumdar, A., "Not Without Engineering," Mechanical Engineering, March (2001), pp.46-49.

4. Krishnan, A., Dujardin, E., Ebbesen, T.W., Yianilos, P.N., Treacy, M.M.J., "Young's Modulus of Single Walled Nanotubes," Physical Review B, Vol. 58, No. 20, (1998), pp. 14 013- 14 019.

5. Salvetat-Delmotte, J.-P. and Rubio, A., "Mechanical Properties of Carbon Nanotubes: A Fiber Digest for Beginners," Carbon, (2002), in press.

6. Lourie, O. and Wagner, H.D., "Evaluation of Young's Modulus of Carbon nanotubes by Micro-Raman Spectroscopy," Journal of Materials Science, Vol. 13, (1998), pp. 2418-2422.

7. Salvetat, J.-P., Briggs, G.A.D., Bonard, J.-M., Bacsa, R.R., Kulik, A., Stockli, Burnham, N.A., and Forro, L., "Elastic and Shear Moduli of Single-Walled Carbon Nanotube Ropes," Physical Review Letters, Vol. 82, No. 5, (1999), pp. 944-947.

8. Sanchez-Portal, D. Artacho, E.,Soler, J.M., Rubio, A. and Ordejon, P., "Ab Initio Structural, Elastic and Vibrational Properties of Carbon Nanotubes," Physical Review B, Vol. 59, (1999), pp. 12678-12688.

9. Hernandez, E., Goze, C., Bernier, P., Rubio, A., "Elastic Properties of C and $B_xC_yN_z$ Composite Nanotubes," Physics Review Letters, Vol. 80, (1998), pp. 4502-4505.

10. Cornwell, C.F. and Wille, L.T., "Elastic Properties of Single-Walled Nanotubes in Compression," Solid State communications, Vol. 101, No. 8, (1997), pp. 555-558.

11. Ruoff, R.S. and Lorents, "Mechanical and Thermal Properties of Carbon Nanotubes, Carbon, Vol. 33, No. 7, (1995), pp. 925-930.

12. Chesnokov, S.A., Nalimova, V.A., Rinzler, A.G., Smalley, R.E. and Fischer, J.E., "Mechanical Energy Storage in Carbon Nanotube Springs," Physical Review Letters, Vol. 82, (1999), pp. 343-346.

13. Gao, G., Cagin, T. and Goddard, W.A., "Energetics, Structure, Mechanical and Vibrational Properties of Single-Walled Carbon Nanotubes,"

Nanotechnology, Vol. 9, (1998), pp. 184-191.

14. Dresselhaus, M.S., Dresselhaus, G. and Saito, R., "Physics of Carbon Nanotubes," Carbon, Vol. 33, No. 7, (1995), pp. 883-891.

15. Yakobson, B.I., Brabec, C.J. and Bernholc, J., "Nanomechanics of Carbon Tubes: Instabilities Beyond Linear Response," Physical Review Letters, Vol. 76, No. 14, (1996), p. 2511.

16. Arepalli, S., Nikolaev, P. and Holmes, W., "Production and Measurements of Individual Single-Wall Nanotubes and Small Ropes of Carbon," Applied Physics Letters, Volume 78, No. 10, (2001).

17. Thess, A., Lee, R., Nikolaev, P., Dai, H., Petit, R.J., Robert, J., Xu, C., Lee, Y.H., Kim, S.G., Rinzler, A., Colbert, D.T. Scuseria, G.E., Toma'nek, Fisher, J. and Smalley, R.E., "Crystalline Ropes of Metallic Carbon Nanotubes," Science, Vol. 273, (1996), pp. 483-87.

18. Saether, E., Frankland, S.J.V. and Pipes, R.B. "Nanostructured Composites: Effective Mechanical Property Determination of Nanotube Bundles," Proceedings of the 43rd AIAA/ASME/ASCE/AHS/ASC Structures, Structural Dynamics and Materials Conference, Denver, (2002).

19. Girifalco, L.A., Hodak, M. and Lee, R.S., "Carbon Nanotubes, Buckyballs, Ropes and a Universal Graphitic Potential," Physical Review B, Vol. 62, No. 19, (2000), pp. 13 104-13 110.

20. Popov, V.N., Van Doren, V.E. and Balkanski, M., "Elastic Properties of Crystals of Carbon Nanotubes," Solid State Communications, Vol. 114, (2000), pp.395-399.

21. Popov, V.N. and Van Doren, V.E., "Elastic Properties of Single-Walled Carbon Nanotubes," Physical Review B, Vol. 61, No. 4, (2000), pp.3078-3084.

Nomenclature

$\mathbf{a_1}$	unit vector
$\mathbf{a_2}$	unit vector
A	constant for SWCN principal Young's modulus calculation
b	C-C bond length (nm)
B	constant for SWCN Young's modulus calculation
E_n	SWCN Young's modulus (GPa)
E_{na}	SWCN Young's modulus in a hexagonal array (GPa)
$E_{\rho a}$	SWCN array specific modulus (GPa)
$E_{\rho n}$	SWCN specific modulus (GPa)
M_w	Atomic weight
m	number of carbon atoms in a_2 direction
n	number of carbon atoms in a_1 direction
N	number of carbon atoms per unit length (atoms/nm)
N_a	Avogadro's number
R_n	SWCN radius (nm)
R_{na}	effective SWCN radius in and hexagonal array (nm)
R_{ne}	effective SWCN radius (nm)
V_a	SWCN volume fraction of the hexagonal array
V_n	SWCN volume fraction
W_n	SWCN array weight fraction
W_n	SWCN weight fraction
Y	graphene Young's modulus (GPa)
Λ	chiral vector function
λ	distance between the SWCN in an hexagonal array (nm)
ν	distance between the SWCN and the adjacent surrounding medium (nm)
ρ_a	SWCN array density (g/cm^3)
ρ_m	SWCN/polymer composite density (g/cm^3)
ρ_n	SWCN density (g/cm^3)
ρ_{na}	SWCN density in a hexagonal array (g/cm^3)
ρ_p	polymer density (g/cm^3)
$\overline{\rho}_a$	SWCN effective array specific gravity
$\overline{\rho}_n$	SWCN effective specific gravity

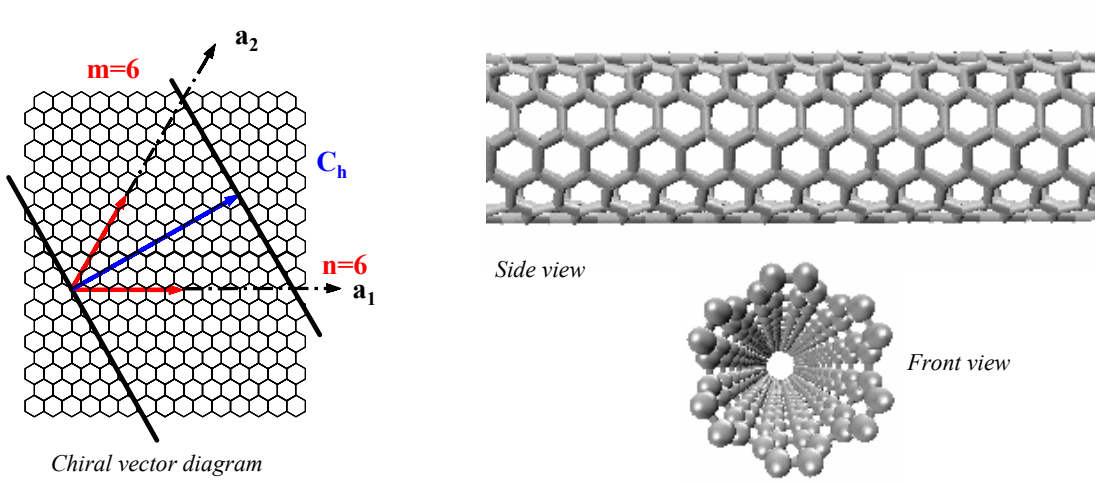

a) Armchair nanotube (6,6)

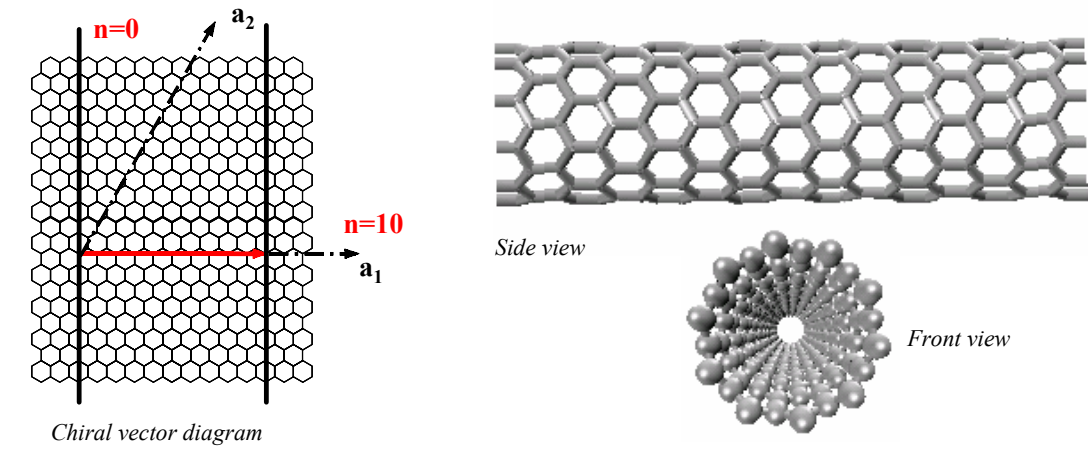

b) Zig zag nanotube (10,0)

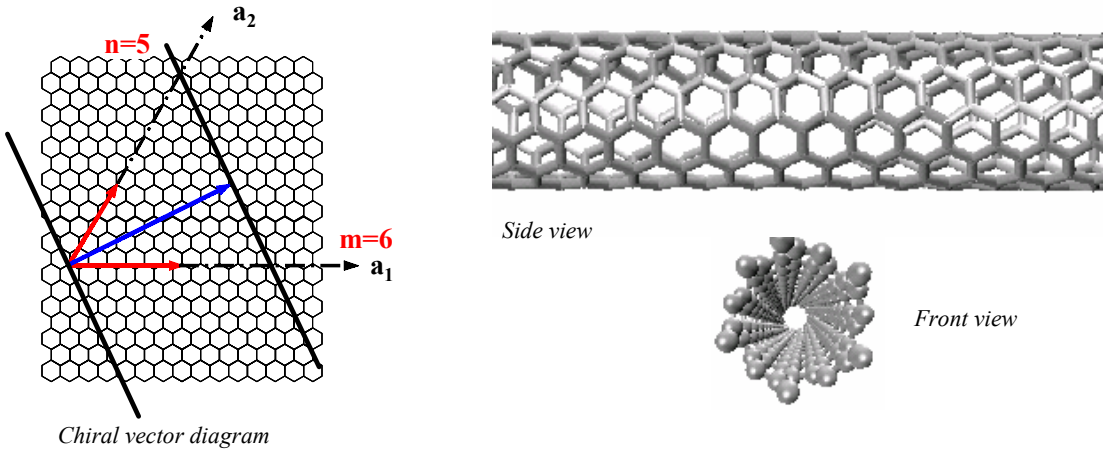

c) Chiral nanotube (6,5)

Figure 1 SWCN structure and example of nanotubes.

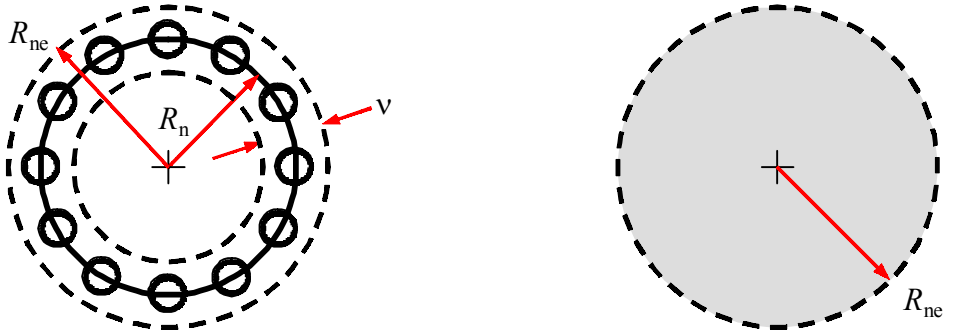

a) Carbon nanotube

b) Effective reinforcement

Figure 2 SWCN nomenclature.

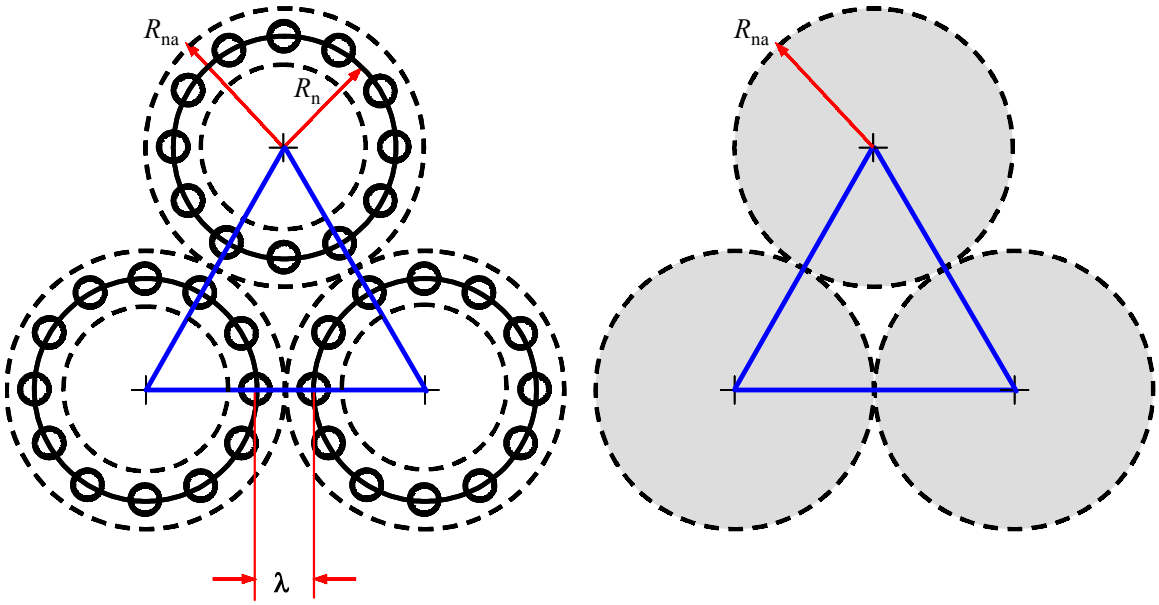

a) Carbon nanotube array

b) Effective reinforcement array

Figure 3 SWCN array nomenclature.

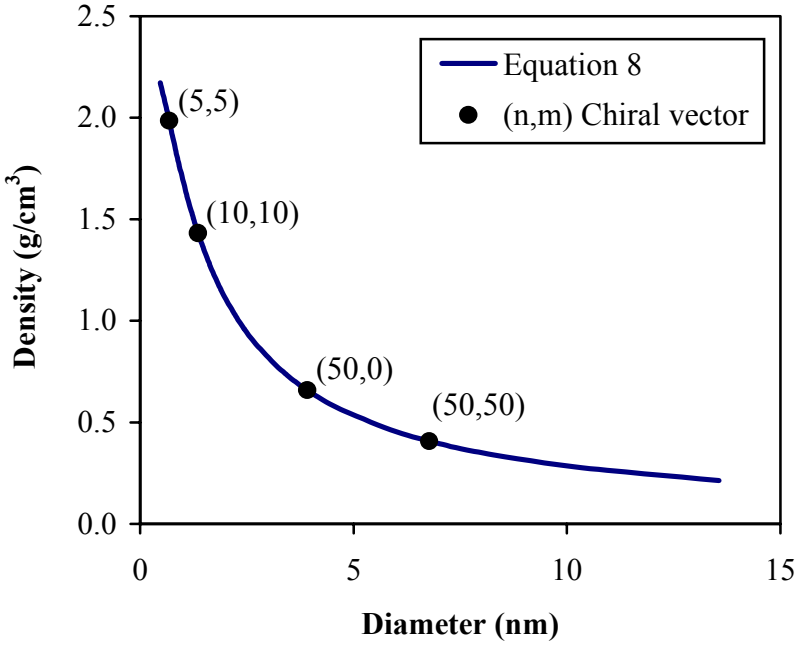

Figure 4 SWCN density versus diameter.

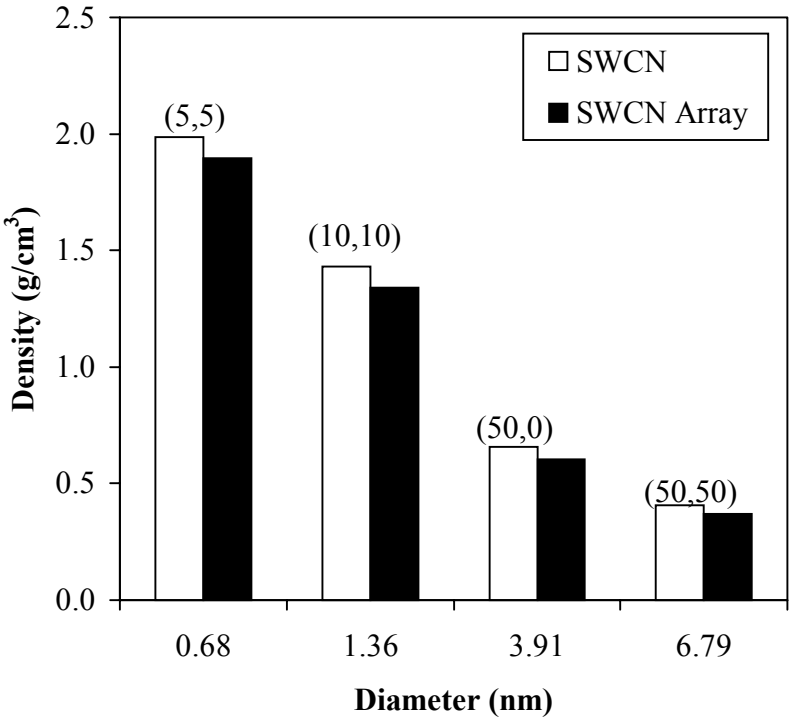

Figure 5 Comparison of SWCN and array densities.

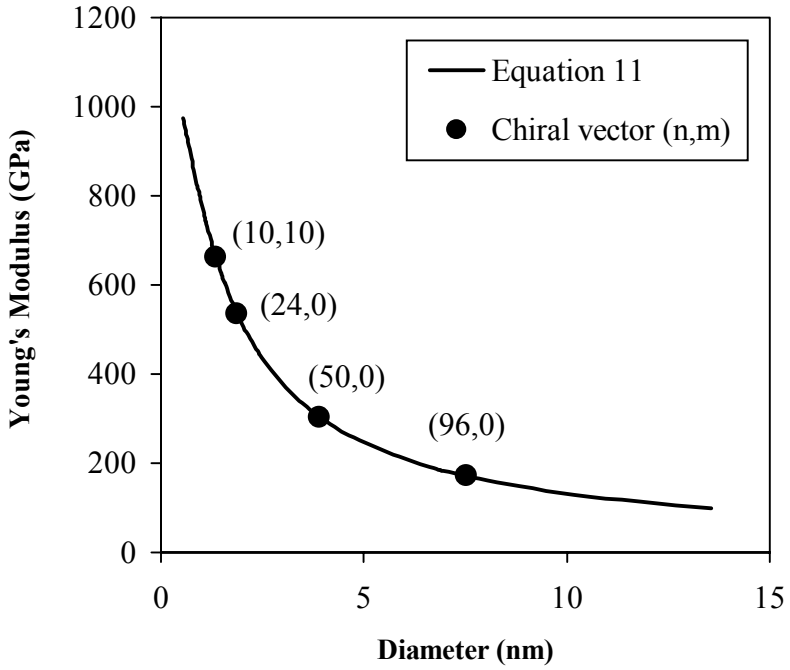

Figure 6 SWCN Young's modulus versus diameter.

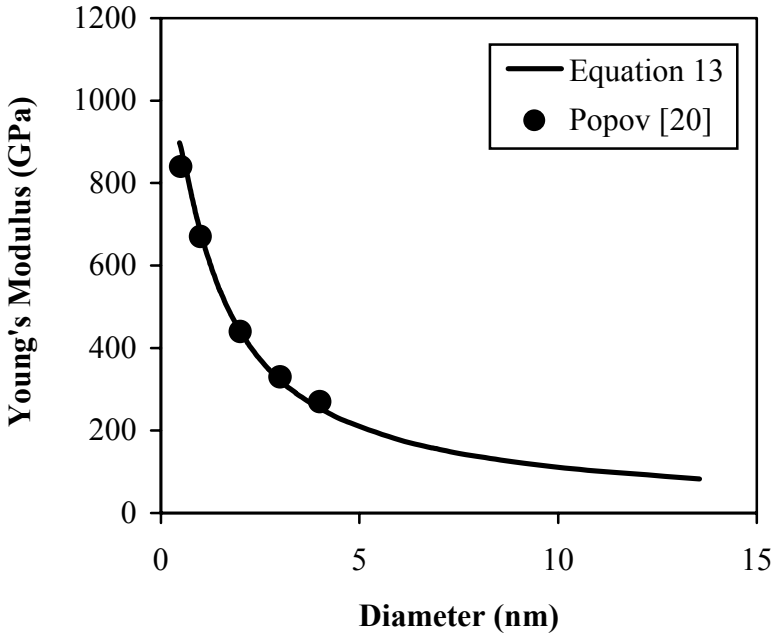

Figure 7 SWCN array Young's modulus versus diameter.

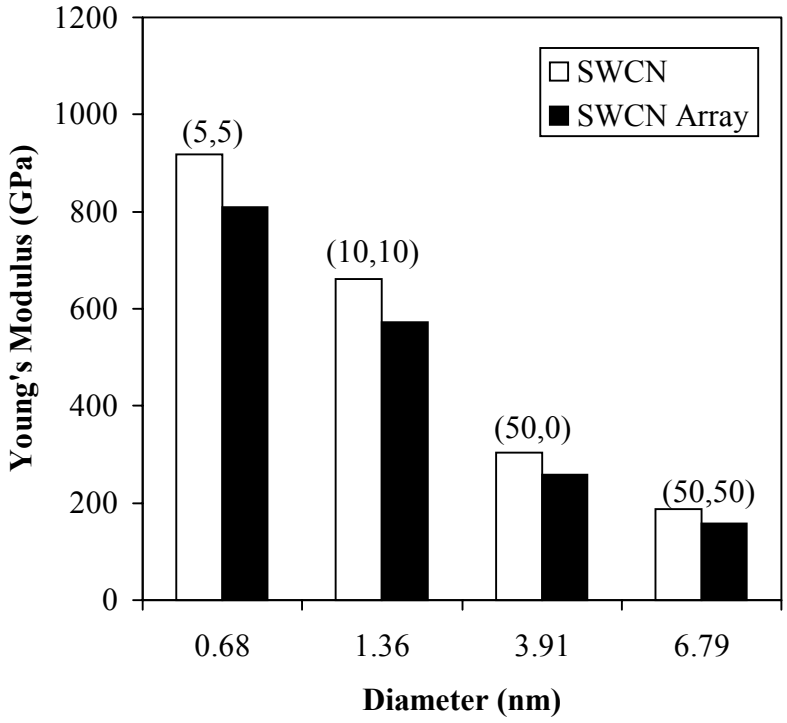

Figure 8 Comparison of SWCN and array Young's modulus.

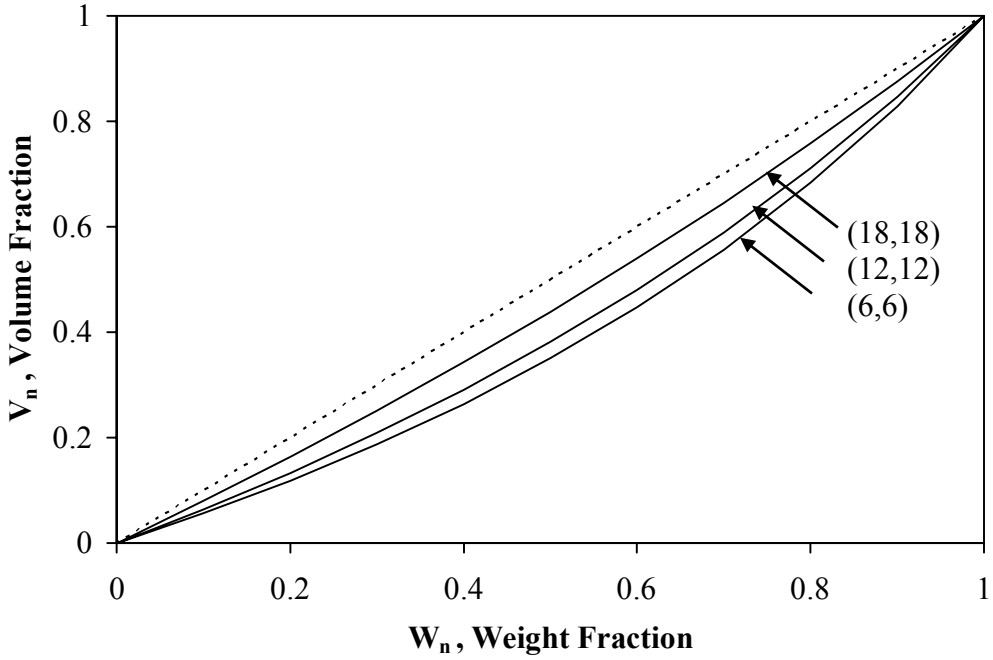

Figure 9 SWCN volume fraction versus weight fraction (polymer density = 1 g/cm^3) .

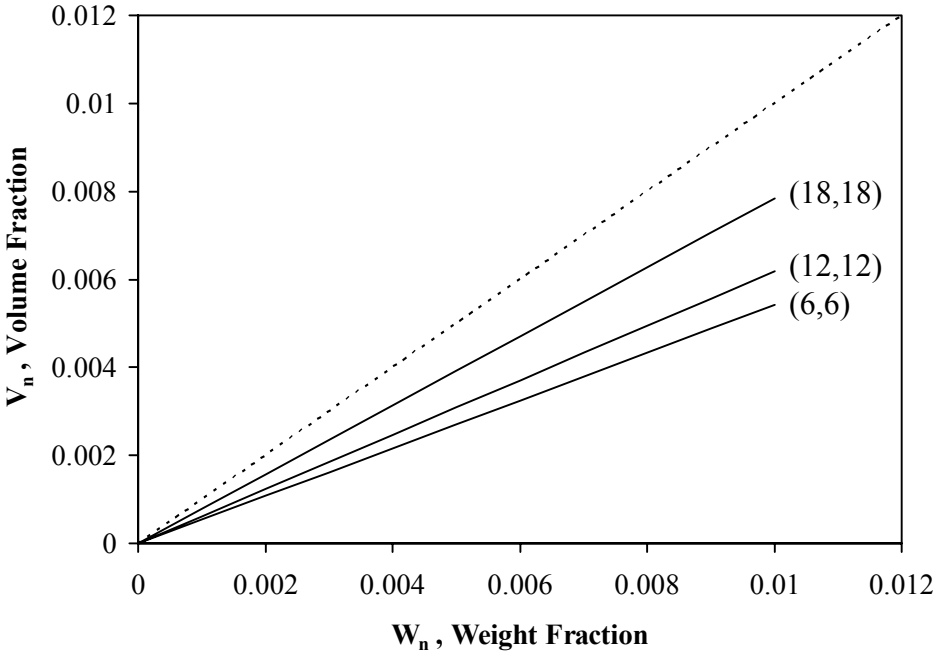

Figure 10 SWCN results at dilute concentrations (polymer density = 1 g/cm^3) .

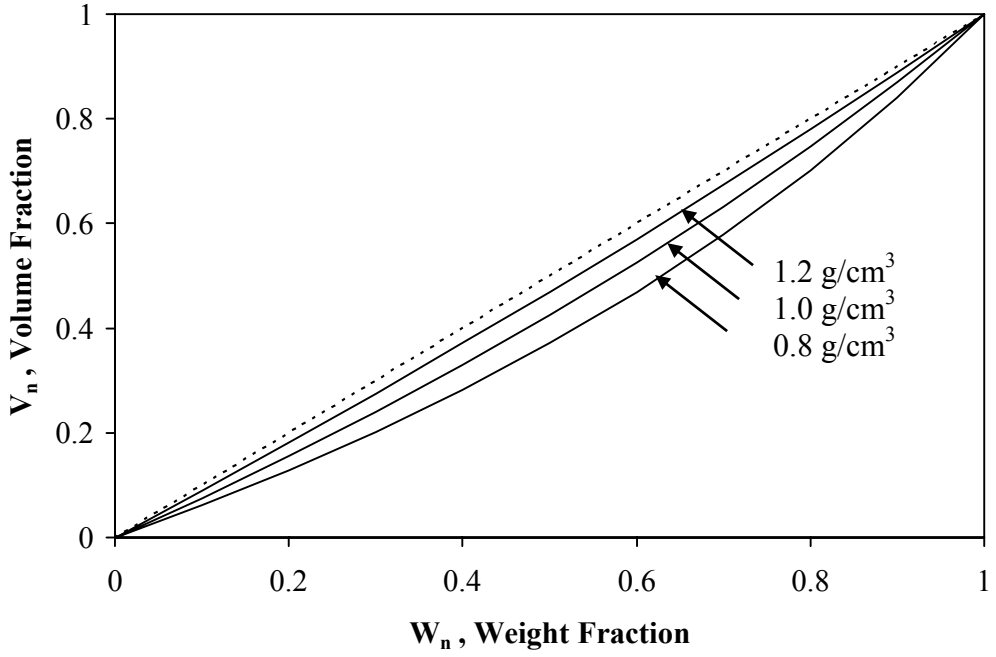

Figure 11 SWCN (10,10) results for different polymer densities.

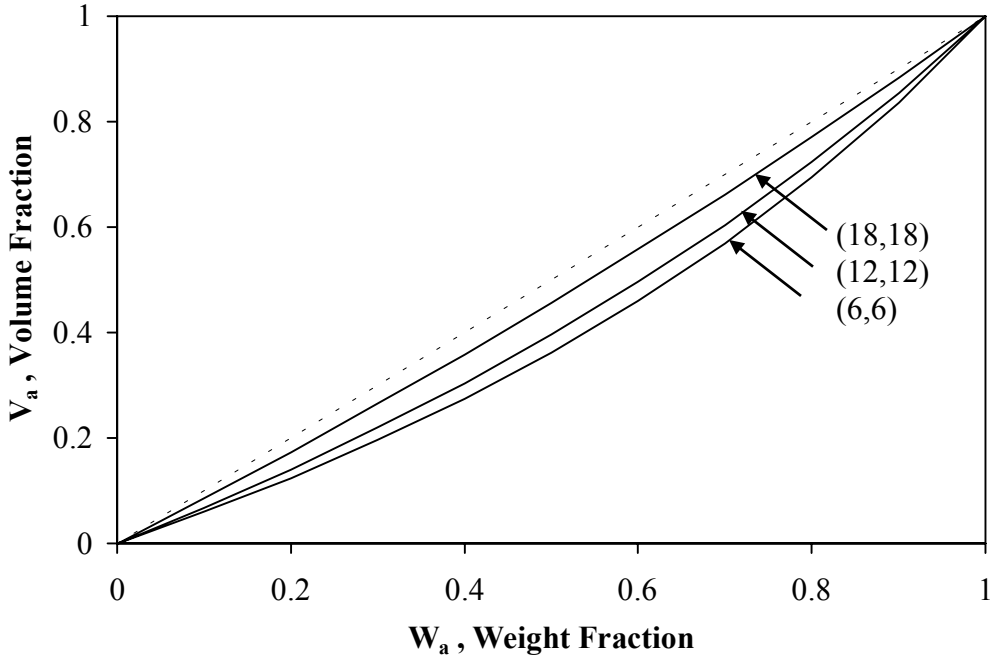

Figure 12 Array volume fraction versus weight fraction (polymer density = 1 g/cm^3).

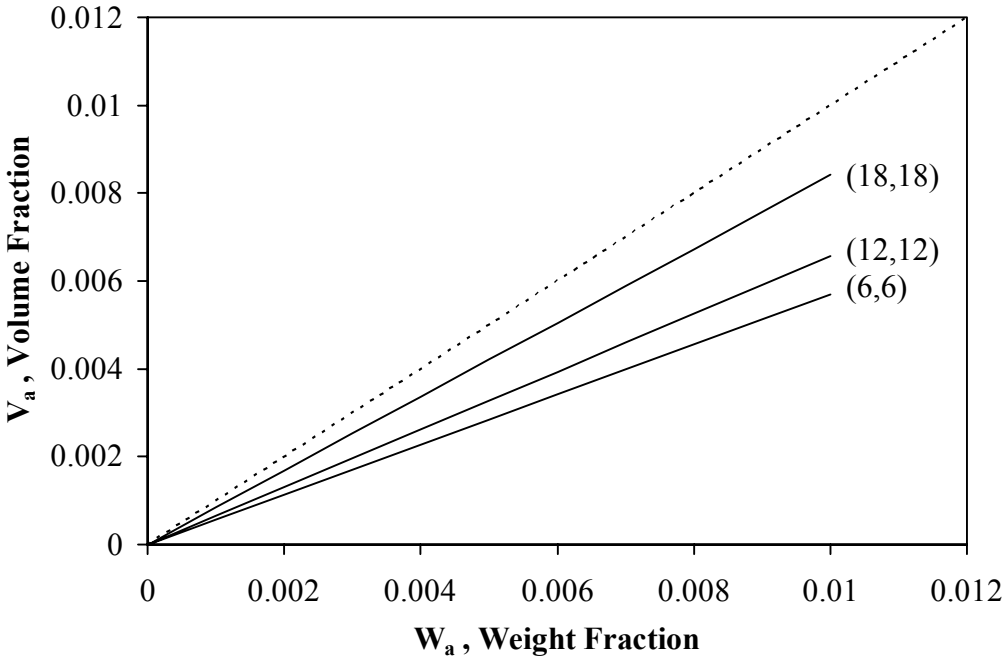

-

Figure 13 Array results at dilute concentrations (polymer density = 1 g/cm^3).

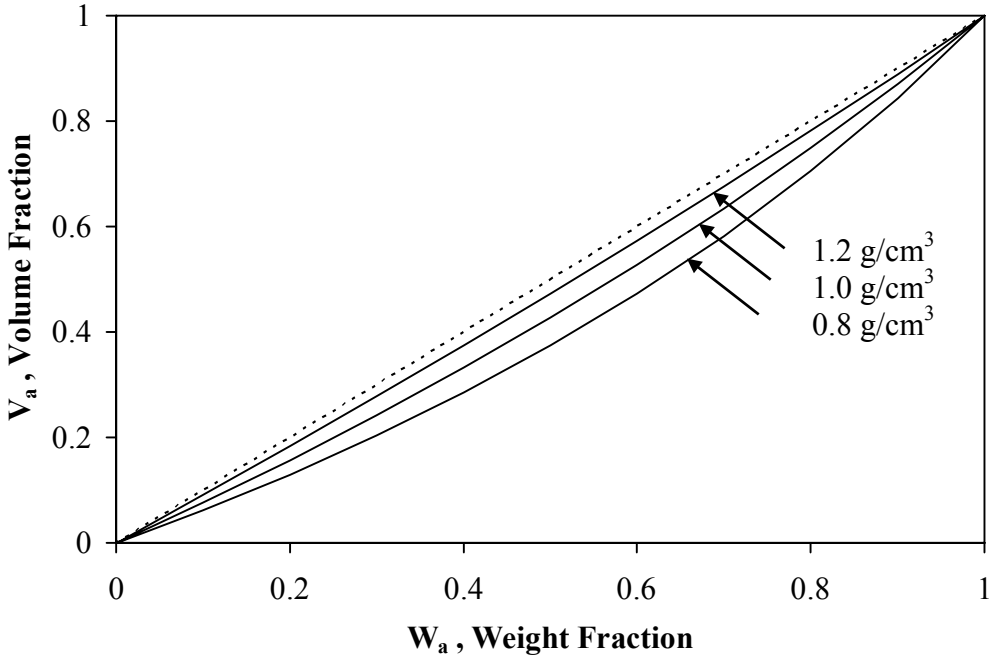

Figure 14 SWCN (10,10) array results for different polymer densities.